

Noise Sources of Closely Installed Subsonic Jets

Wang, Zhong-Nan; Harris, Brandon; Tyacke, James; Tucker, Paul

DOI:

[10.2514/6.2024-3313](https://doi.org/10.2514/6.2024-3313)

License:

None: All rights reserved

Citation for published version (Harvard):

Wang, Z-N, Harris, B, Tyacke, J & Tucker, P 2024, Noise Sources of Closely Installed Subsonic Jets. in *30th AIAA/CEAS Aeroacoustics Conference* ., AIAA 2024-3313, AIAA/CEAS Aeroacoustics Conference, American Institute of Aeronautics and Astronautics Inc. (AIAA), 30th AIAA/CEAS Aeroacoustics Conference (2024), Rome, Italy, 4/06/24. <https://doi.org/10.2514/6.2024-3313>

[Link to publication on Research at Birmingham portal](#)

General rights

Unless a licence is specified above, all rights (including copyright and moral rights) in this document are retained by the authors and/or the copyright holders. The express permission of the copyright holder must be obtained for any use of this material other than for purposes permitted by law.

- Users may freely distribute the URL that is used to identify this publication.
- Users may download and/or print one copy of the publication from the University of Birmingham research portal for the purpose of private study or non-commercial research.
- User may use extracts from the document in line with the concept of 'fair dealing' under the Copyright, Designs and Patents Act 1988 (?)
- Users may not further distribute the material nor use it for the purposes of commercial gain.

Where a licence is displayed above, please note the terms and conditions of the licence govern your use of this document.

When citing, please reference the published version.

Take down policy

While the University of Birmingham exercises care and attention in making items available there are rare occasions when an item has been uploaded in error or has been deemed to be commercially or otherwise sensitive.

If you believe that this is the case for this document, please contact UBIRA@lists.bham.ac.uk providing details and we will remove access to the work immediately and investigate.

Noise sources of closely installed subsonic jets

Zhong-Nan Wang¹, Brandon Harris²
University of Birmingham, Birmingham, England B15 2TT, UK

James Tyacke³
Brunel University London, Uxbridge, England UB8 3PH, UK

and Paul Tucker⁴
University of Cambridge, Cambridge, England CB3 1PZ, UK

Emitted noise of an installed jet is significantly louder, compared to an isolated jet. When the jet is installed close to a solid surface, nonlinear jet-surface interactions occur and modify the jet turbulence in addition to the linear potential field interactions. In this paper, the noise sources are decomposed into quadrupole sources due to turbulent mixing and dipole sources due to the unsteady loadings on the surface. The change of these two sources due to close installation is first characterised in the near-field and their contribution to the far-field noise is then quantified. The quadrupole sources and noise are examined using Goldstein’s acoustic analogy, whilst dipole noise is studied with the Amiet approach to model trailing edge scattering of evanescent hydrodynamic waves. The methods are first validated in a plate-jet configuration and then applied to analyze the noise sources of a closely installed jet-wing configuration. The results show that the increased quadrupole source primarily contributes to the installation noise at the polar angle of around 30 degrees, while the dipole source is responsible for the installation noise at the higher polar angles.

Nomenclature

a	=	speed of sound
c_0	=	chord length
D	=	nozzle diameter
H	=	vertical distance between the jet centre line and the plate underneath
L	=	axial distance between jet exit and plate trailing edge
W	=	half-width of the flat plate
U	=	time-averaged velocity
\mathbf{u}	=	velocity fluctuations (u_1, u_2, u_3)
M	=	Mach number
k	=	acoustic wavenumber, ω/a
ω	=	angular frequency
(x, y, z)	=	Cartesian coordinates
(x, r, θ)	=	cylindrical coordinates, <i>i.e.</i> axial, radial and azimuthal coordinates

I. Introduction

AIRCRAFT noise is a major concern to communities neighbouring airports [1]. Jet noise from aeroengines is still the dominant component when an aircraft is taking off. High-bypass-ratio engines reduce jet noise by lowering the jet exit speed. However, when the bypass ratio is further increased, the jet engine has to be installed closer to the wing. This significantly intensifies jet noise due to the strong interaction between the jet and the wing. This is normally referred to as installed jet noise and usually occurs in the low-frequency range. Historically, the extra noise due to the

¹ Lecturer, College of Engineering and Physical Sciences; Visiting Academic Fellow, Department of Engineering, University of Cambridge; Member AIAA. z.n.wang@bham.ac.uk (Corresponding Author)

² Research Student, College of Engineering and Physical Sciences.

³ Senior Lecturer, Department of Mechanical and Aerospace Engineering; Member AIAA

⁴ Rank Professor of Engineering, Department of Engineering; Associate Fellow AIAA.

wing installation was first noticed by Bushell [2] by comparing the in-flight installed jet with a static isolated jet for a full-scale aircraft. The characteristics of this installed jet have been studied extensively by experimentalists [3-5]. The directivity of installation noise is found to be dipole-like and it is also sensitive to the distance from the jet to the solid surface and the distance from the jet exit to the surface trailing edge. To understand the mechanism, Ffowcs Williams and Hall in 1970 observed that the far-field low-frequency noise can be amplified when a turbulent flow is next to a surface [6]. They attributed this amplification to the hydrodynamic scattering near the solid surface edge. Lyu and Dowling confirmed this theory and developed a reliable prediction model [7] based on hydrodynamic wave scattering. It demonstrated that the far-field sound amplification can be accurately predicted by incorporating the scattering of the near-field hydrodynamic evanescent wave using the Amiet approach [8]. It should be noted that this prediction method is used when the solid surface sits in the irrotational flow region, therefore regarded as a linear mechanism of noise generation for installed jets. However, when the solid surface moves close to the surface, such as in Ultra-High Bypass-Ratio engine installation, the nonlinear interaction between the jet and solid surface begins to increase. The jet mixing shear layer near the solid surface is significantly altered. The jet mixing noise source is likely to be modified in a closely-installed configuration [9]. This could further lead to the change in far-field noise. There is still a lack of understanding in this scenario, which puts in question the noise generation mechanism of installed jets for realistic applications.

In this paper, we will investigate the jet-surface interactions and their generated noise in closely installed jets. Two noise sources, i.e. quadrupole sources of turbulent mixing in the jet plume and dipole sources of unsteady loading on the solid surface, are examined to evaluate the impact of the close installation. Their contribution to the far-field installation noise will be quantified by comparing it with the isolated jet.

II. Methods

A. Flow and acoustics predictions

LES is used to capture large-scale turbulence that is responsible for noise generation. Accurate LES requires a numerical scheme with low dissipation characteristics to resolve approximately 90 percent of flow energy. A non-dissipative numerical scheme that preserves the kinetic energy [10] was used in our simulation to ensure the computation is stable without any artificial dissipation. The scheme is blended with 4th order Laplacian smoothing and gradually stretching grids towards the computational boundary to prevent numerical reflection. As to the turbulence modelling, a RANS layer is used near the wall to cover the inner part of boundary layer, while LES is used to resolve the outer part of boundary layer and turbulent jet plume. The RANS layer is blended with the LES region using a specially designed blending function based on modified wall distance [11]. In our simulation, the SA RANS model [12] and the WALESGS model [13] are used to treat turbulence in different regions. The full details of the turbulence modelling can be found in the reference [14] for jet-plate configuration and the reference [15] for jet-wing configuration.

To predict the far-field acoustics, FW-H integration is performed over a time series of flow data on the near-field FW-H surfaces. Three FW-H surfaces are placed with increased radial positions around the jet plume and plate/wing. This is to ensure the surfaces lie in the irrotational region and enclose all the quadruple sources so that a robust and accurate far-field sound prediction can be obtained. The detail of the near-field FW-H surface placement can also be found in our previous publications [14, 16].

B. Noise sources analysis

If the FW-H integration is performed on the solid surface, the contribution of installed jet noise breaks down into two categories: quadrupole sources due to turbulent mixing and dipole sources due to the unsteady loadings on solid surfaces.

$$PSD_{total} = PSD_{quad} + PSD_{dipole}$$

1. Quadrupole source: Goldstein's acoustic analogy

The quadrupole source can be accurately studied with Goldstein's acoustic analogy [17] that accounts for the mean-flow refraction for acoustics propagation. The noise source is characterized by space-time correlations of Reynolds stress tensors and it can be modelled by Gaussian functions [18]. When they are integrated with Green's functions, the prediction of far-field noise is obtained as below

$$PSD_{Quad}(\mathbf{x}, \omega) = c^4 \int_{V_y} \int_{V_{\delta y}} \hat{R}_{ijkl}(\mathbf{y}; \delta \mathbf{y}, \omega) I_{ijkl}(\mathbf{x}, \mathbf{y}; \delta \mathbf{y}, \omega) d^3 \delta y d^3 y$$

where $PSD_{Quad}(\mathbf{x}, \omega)$ is the power spectral density of quadrupole noise at the observer location \mathbf{x} , $\hat{R}_{ijkl}(\mathbf{y}; \delta\mathbf{y}, \omega)$ is the cross spectra density of the 4th order space-time velocity correlation $R_{ijkl}(\mathbf{y}; \delta\mathbf{y}, \tau)$ with space separation $\delta\mathbf{y}$ and time delay τ , which characterises the sound source at the location \mathbf{y} in the jet plume. $I_{ijkl}(\mathbf{x}, \mathbf{y}; \delta\mathbf{y}, \omega)$ is the Green's function that propagates the flow energy in the source to the far-field as acoustics.

2. Dipole sources: Amiet's trailing edge scattering model

The hydrodynamic waves in the jet shear layer are evanescent and inaudible as they decay exponentially away from the jet. When a trailing edge is present in installed jets, the evanescent wave will be scattered and the pressure fluctuations can be propagated to the far-field as sound. The far-field noise generated by this trailing edge scattering is used here to approximate dipole noise. It can be predicted using the Amiet approach [8] with the input of evanescent waves [7], shown below

$$PSD_{Scat}(\mathbf{x}, \omega) = \left[\frac{\omega x_3}{c_0 S_0^2} \right]^2 \left\{ \left| \frac{\Gamma(c, \mu, \mu_A)}{\mu_A} \right|^2 \frac{e^{-2H\gamma_c} PSD(\omega, r_0)}{2\gamma_c^2 K_0^2(\gamma_c r_0)} \right\}_{k_2=0}$$

In the above, $PSD(\omega, r_0)$ is the power spectral density of pressure fluctuations at the same axial location of the trailing edge and the radial location of r_0 . $K_0^2(\gamma_c r_0)$ is the Bessel function that describes the radial decay of evanescent waves with a rate $\gamma_c = \sqrt{(k_1 \beta + kM)^2 - k^2}/\beta$. The axial wave number of evanescent waves, k_1 , is obtained such that the reduced spectra $\frac{PSD(\omega, r_0)}{K_0^2(\gamma_c r_0)}$ is independent of radial location r_0 where evanescent waves dominate.

III. Validation: Jet-Plate Interaction Noise

A canonical case is used to validate the method of noise source analysis. The configuration consists of a single stream jet placed under a flat plate. The trailing edge of the plate is placed at 4 diameters D_j downstream of the jet exit and 1 diameter away from the nozzle centerline. The LES has been performed on this configuration with far-field noise predicted with the FW-H approach [14]. Both near-field turbulence and far-field noise have been accurately captured. Figure 1 shows the flow field of axial velocity and turbulent kinetic energy (TKE) for both isolated and installed cases. Compared to the isolated jet, the installed jet slightly touches the trailing edge of the plate. Both jet velocity and turbulence are barely affected by the plate. This indicates that the interaction between jet and plate lies in the linear regime. This is used to validate the methods for source analysis, *i.e.* the Goldstein acoustic analogy for quadrupole sources and the Amiet trailing edge scattering model for dipole sources.

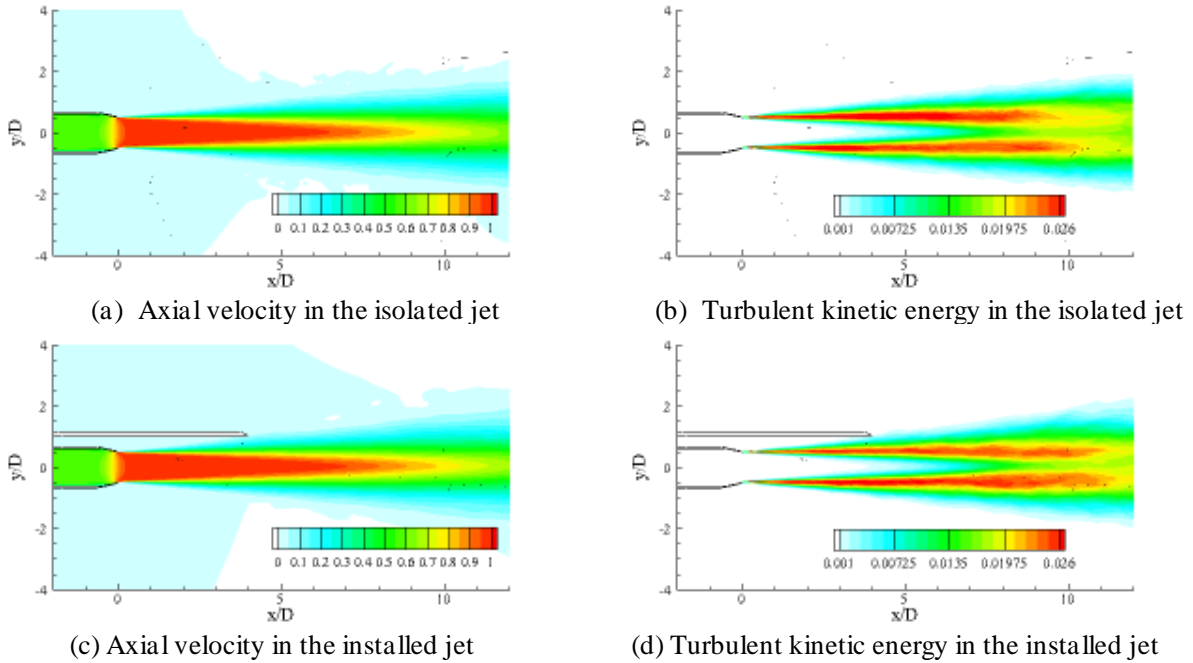


Figure 1 Time-averaged velocity and turbulent kinetic energy (TKE) at the plane cutting through the jet centerline for the isolated and installed jets with the relative position to the plate of $H/D = 1, L/D=4$

The Goldstein acoustic analogy is used for investigating the noise generation of quadrupole sources and predicting its far-field noise. To avoid the complexity of calculating space-time correlation directly from LES data, the turbulent kinetic energy and time-averaged vorticity obtained from the LES are used to calculate the source amplitudes and (time and length) scales for constructing the Gaussian function that models the 4th-order space-time correlation of velocities for quadrupole noise sources [19]. It has been verified that the TKE and vorticity-based space-time correlations are consistent with those directly computed from LES data. The far-field noise is predicted by integrating the noise sources, calculated for both isolated and installed jets, with Green's functions that are based on the jet mean flow. With the knowledge that the scattering of quadrupole sources by trailing edge is insignificant and acoustic reflection/shielding only affects acoustics at high frequencies [7], the free-field Green's function is used as an approximation for quadrupole noise prediction of installed jets. Figure 2 shows the prediction of quadrupole noise for both isolated and installed jets at two representative polar angles under the plate. The experimental data is used as a reference to validate the accuracy of the prediction using Goldstein's acoustic analogy. The far-field noise of isolated jets is entirely from quadrupole sources and the noise prediction using Goldstein's acoustic analogy agrees well with the experimental measurement up to around $St=2$. The quadrupole noise of the installed jet stays extremely close to that of isolated jets, indicating that the quadrupole sources have not been affected by the installation for this jet-plate configuration of $H/D=1.00$ and $L/D=4.00$.

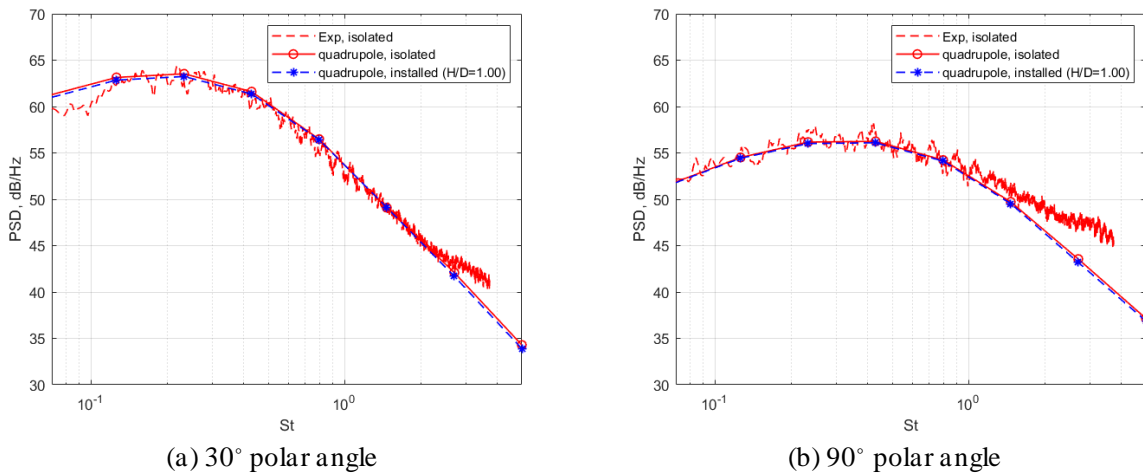


Figure 2 Quadrupole noise at the polar angles of 30° and 90° from the downstream direction (under the plate for installed jets) for both isolated and installed jets

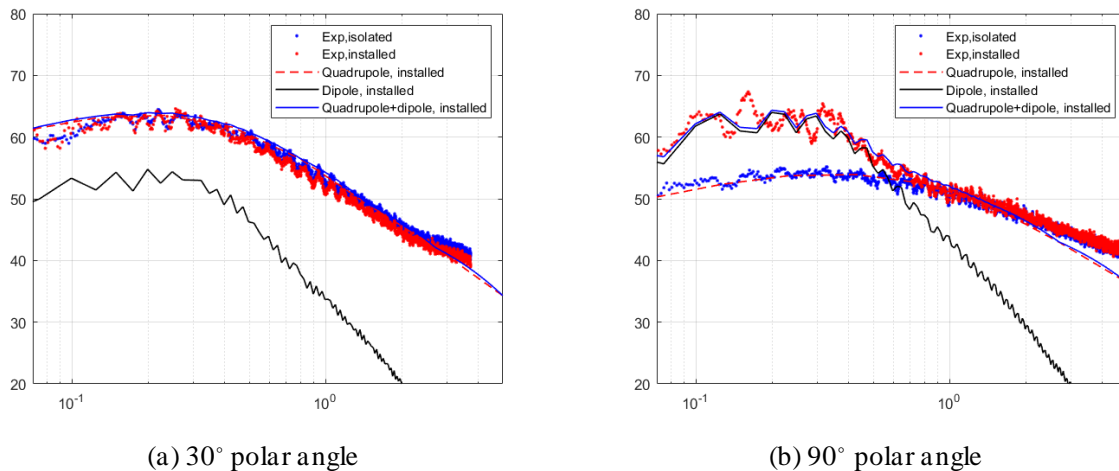


Figure 3 Far-field noise from quadrupole and dipole sources at the polar angles of 30° and 90° from the downstream direction (under the plate for installed jets) for both isolated and installed jets

In addition to the quadrupole noise, the noise generated by dipole sources is predicted by scattering the evanescent waves at the trailing edge of the plate, as shown in Figure 3. The total noise is obtained by adding the dipole noise to the quadrupole noise. At the polar angle of 30° (from the jet direction), the dipole noise is insignificant, which is about

10 dB lower than the quadrupole noise, so the installed jet noise is almost the same as that of isolated jet noise. As the polar angle increases, the dipole noise becomes more evident compared to that of the quadrupole. At the polar angle of 90° , the dipole noise, generated by trailing scattering becomes dominant, is about 10 dB larger than the quadrupole noise. The far-field noise of installed jets can be well predicted by adding the noise from quadrupoles and dipoles together. The predicted noise is in excellent agreement with experimental data. This shows the validity of the proposed methods for quadrupole and dipole source analysis.

IV. Application: Jet-Wing Interaction Noise Sources

The methods used for noise source analysis of the jet-plate configuration will be used here to investigate the installation noise sources of an industrially relevant jet-wing configuration, which is an ultra-high bypass ratio (UHBR) engine nozzle installed closely under a three-dimensional wing. The flows and acoustics have been well predicted using hybrid LES-RANS and FWH methods [16, 20]. Figure 4 reviews the flow field of velocities and TKE for both isolated and installed jets. The wing is closely placed above the jet nozzle, leading to significant interactions with the turbulent jet. As shown in the axial velocities, the jet plume has been deflected by the wing. Compared to the isolated jet, the TKE in the upper shear layer has been modified by the wing. The TKE firstly decays under the wing and then amplifies downstream of the wing due to the jet-wing interactions. This enhanced turbulence is expected to have an impact on turbulent mixing noise, which will be discussed in the section below.

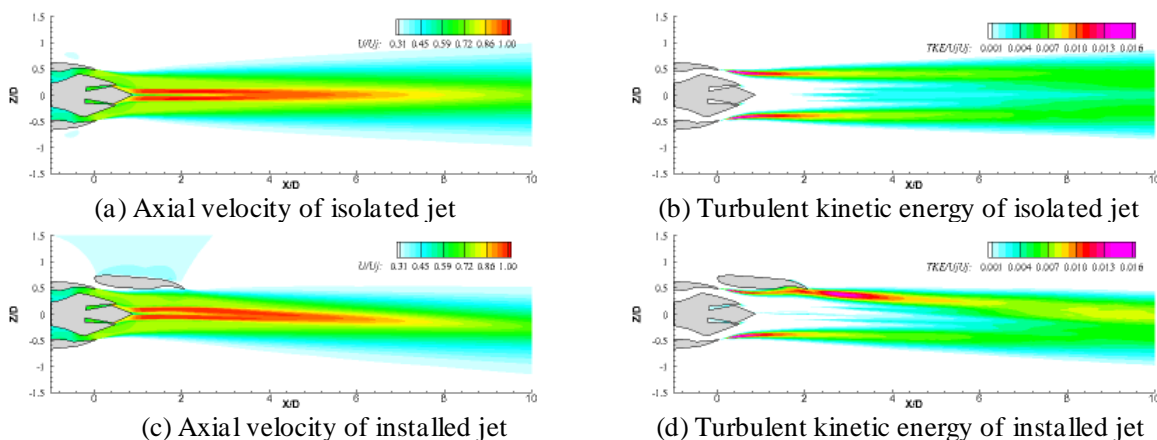


Figure 4 Time-averaged flow field of an ultra-high bypass-ratio nozzle jet installed under a wing

A. Quadrupole sources

The quadrupole source due to turbulence mixing is characterised by the space-time correlations, $R_{ijkl}(\mathbf{y}; \delta\mathbf{y}, \tau)$, in the Goldstein's acoustic analogy. Among all the components, $R_{1111}(\mathbf{y}; \delta\mathbf{y}, \tau)$, which is the four-order correlation of axial velocities, is dominant. Figure 5 shows the amplitudes of R_{1111} , which is at zero spatial separations, $\delta\mathbf{y}=\mathbf{0}$, and at zero time delay $\tau = 0$, for both isolated and installed jets. Similar to TKE, the noise source amplitude has been significantly amplified directly downstream of the wing by the jet-wing interactions. The increase of amplitude peaks directly downstream of the wing and also further extends downstream in the upper jet shear layer. However, it is not necessary that all the increased energy in the noise source can be propagated to the far-field as acoustics with the same efficiency.

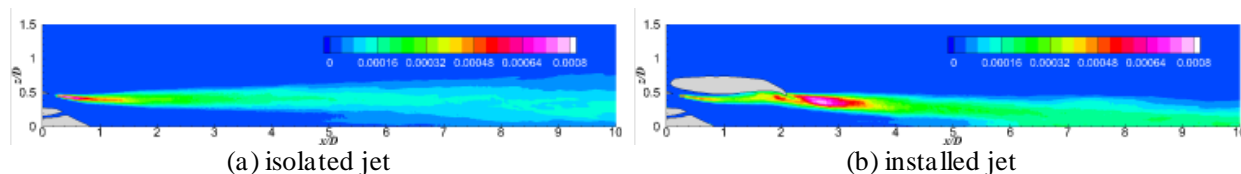


Figure 5 Amplitude of the dominant component of space-time correlations, $R_{1111}(\mathbf{y}; \delta\mathbf{y} = \mathbf{0}, \tau = 0)$

The source contribution at the location of \mathbf{x} to the far-field noise of the frequency ω at the observer's location \mathbf{y} can be quantified by integrating the space-time correlation $R_{ijkl}(\mathbf{y}; \delta\mathbf{y}, \tau)$ with the Green's function $I_{ijkl}(\mathbf{x}, \mathbf{y}; \delta\mathbf{y}, \omega)$ over the volume within which the source remains correlated.

$$S_q(\mathbf{x}, \mathbf{y}; \omega) = \int_{V_{\delta y}} \hat{R}_{ijkl}(\mathbf{y}; \delta \mathbf{y}, \omega) I_{ijkl}(\mathbf{x}, \mathbf{y}; \delta \mathbf{y}, \omega) d^3 \delta \mathbf{y}$$

This is referred to as effective quadrupole sources, which is the inner integration of the equation used for predicting the far-field noise. Figure 6 shows the effective noise sources for the observer’s polar angle of 90° at two frequencies, St=0.43 and 1.47. The noise source that contributes to the same observer location can vary with the frequency. With increasing frequencies, the effective sources are more concentrated towards the jet nozzle. This suggests that the turbulent mixing close to the nozzle exit, which occurs at finer scales, is responsible for the high-frequency noise generation, while the region of effective sources for low-frequency noise extends further downstream. This indicates that large-scale turbulence in the downstream plays an important role in generating low-frequency noise. Compared to the isolated jet, the installation has increased the effective quadrupole sources at both frequencies downstream of the wing.

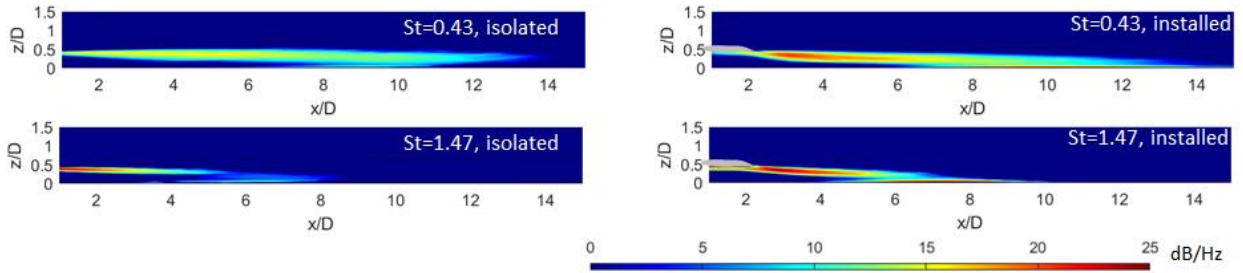


Figure 6 Effective quadrupole noise sources with varying frequencies, St=0.43 and 1.47, at the observer’s polar angle of 90°

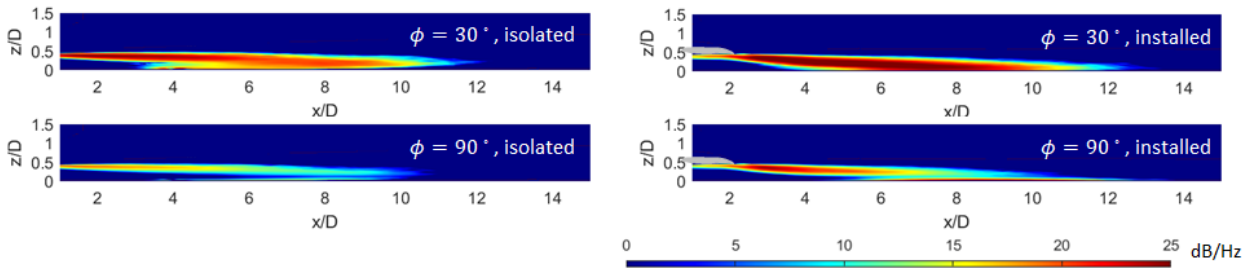


Figure 7 Effective quadrupole noise sources with St=0.8 at the observer’s polar angles of 30° and 90°

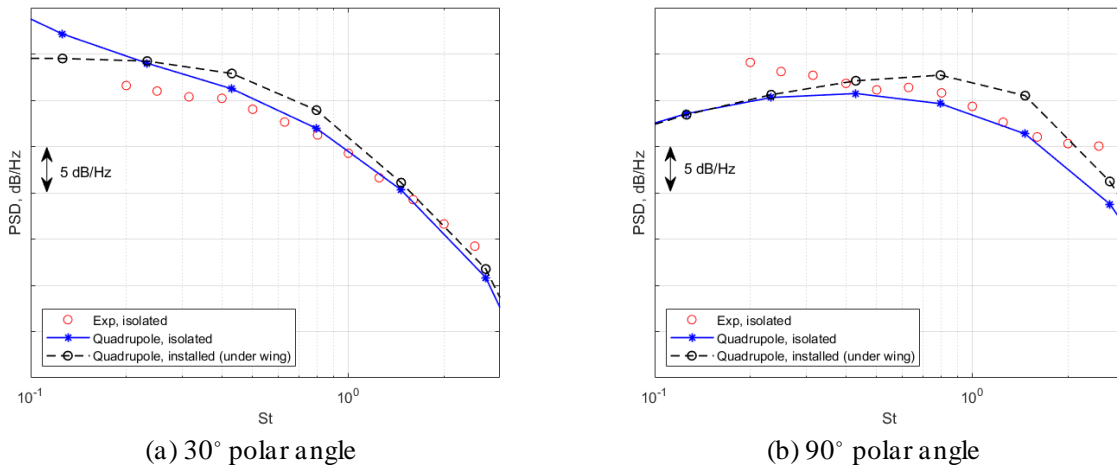


Figure 8 Quadrupole noise at the polar angles of 30° and 90° for both isolated and installed jets (under the wing)

At the frequency of St=0.8, the effective noise source also changes with observer angle, as shown in Figure 7. The amplitude of effective quadrupole sources shows that turbulent mixing in the jet plume is more effective in radiating acoustics at the polar angle of 30° than at the polar angle of 90°. Compared to the effective sources for the 30° polar

angle, the extent of the noise source for the 90° polar angle slightly moves closer to the jet nozzle. This indicates that the noise generation at larger observer angles intends to occur near the nozzle at small turbulence scales. The installation has amplified the effective noise sources for both of the observer's polar angles. The amplification occurs downstream of the wing and also extends further downstream.

When the effective quadrupole source is further integrated over the entire jet plume, the far-field noise generated by turbulent mixing is predicted. Figure 8 shows the comparison of the quadrupole noise of both isolated and installed jets. Different from that of the jet-plate configuration, the noise amplification due to quadrupole sources caused by turbulence is evident for the closely installed jet-wing configuration. The noise of the isolated jet predicted using the Goldstein's acoustic analogy is compared with the experimental data, showing a fairly good agreement. The quadrupole noise amplification due to the installation increases with polar angles. The peak increase is 2-3 dB at the polar angle of 30° and 4-5 dB at the polar angle of 90° . At higher polar angles, the noise amplification tends to occur at higher frequencies. However, the noise amplification caused by increased quadrupole sources is still not enough to explain the observed noise increase due to installation. The contribution of dipole sources will be discussed in the following section.

B. Dipole sources

The dipole source is approximated by the scattering of evanescent hydrodynamic waves at the trailing edge of the wing. The evanescent hydrodynamic waves are coherent in both space and time and can be elucidated using spectral proper orthogonal decomposition (SPOD) [21]. Figure 9 shows the leading SPOD modes of pressure fluctuations for the first two azimuthal modes. The coherent structures in the jet shear layer are in the form of wave packets [22]. Their acoustic emission efficiency is relatively low in the subsonic jet as they decay exponentially in the radial direction from the jet centerline. When a solid surface edge is placed near the jet, the evanescent waves are scattered by the trailing edge and become efficient noise emitters [7].

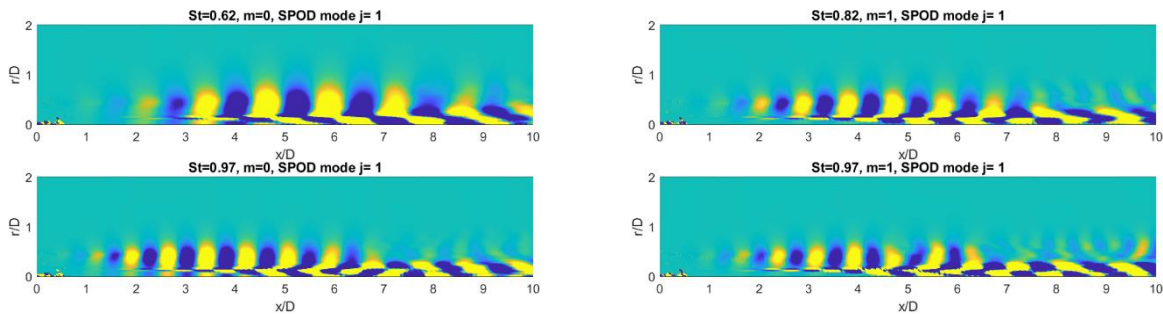


Figure 9 Leading SPOD modes at the first two azimuthal modes of pressure fluctuations $m = 0$ and 1 at the frequencies of $St=0.62$ and 0.97

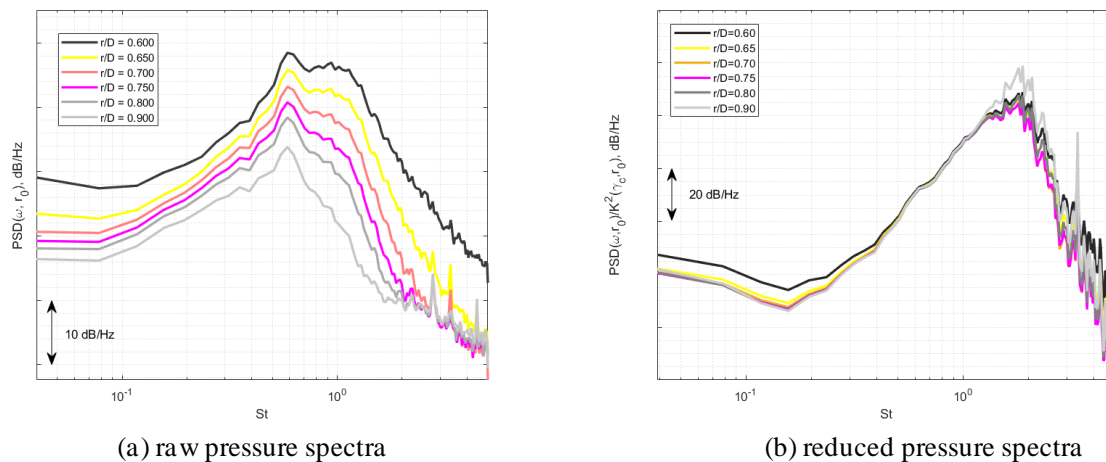


Figure 10 Raw and reduced spectral power density (PSD) of pressure fluctuations at various radial locations of the isolated jet

This scattering noise can be predicted with the input of the spectra of the evanescent waves. Figure 10(a) shows the spectra of pressure fluctuations with increasing radial locations at the same axial position of the trailing edge. The

peak of spectra corresponds to the evanescent waves whose spectra power density (PSD) decays exponentially in radius following the Bessel function $K_0^2(\gamma_c r_0)$ while high-frequency PSD, primarily contributed by acoustic waves, decays slower following $1/r^2$. When the PSD is scaled by $1/K_0^2(\gamma_c r_0)$, the reduced PSD is obtained and it should become independent of radial locations in the frequency region where the evanescent waves dominate. The spectra at $r/D=0.6$ and 0.9 are outliers as they are contaminated by the stochastic turbulent and acoustic fluctuations respectively. The spectra between $r/D=0.6$ and 0.9 collapse well into one curve, as shown in Figure 10(b). The reduced spectra are then used to predict the far-field noise.

Figure 11 summarises the far-field noise contribution from both dipole and quadrupole sources at the two representative polar angles. The total noise is predicted by adding the noise of quadrupoles and dipoles together. To illustrate the relative contributions of quadrupoles and dipoles to the total installation noise, the quadrupole noises of both isolated and installed jets are added to the dipole noise that is calculated based on trailing edge scattering. At the polar angles of 30° , the noise generated by dipole sources is insignificant compared with the quadrupole noise. When the dipole noise is added to the quadrupole noise of the installed jet, the installed jet noise has been well recovered and agrees with the experimental data. Compared to the total noise by adding the dipole noise to the quadrupole source of isolated jets, the noise increase at intermediate frequencies indicates that the installation noise is primarily contributed by the increased quadrupole source due to the enhanced turbulence mixing because of jet-wing interactions. However, the generation mechanisms of installation noise become different at the polar angle of 90° . The quadrupole noises of both isolated and installed jets are negligible compared to the dipole noise. When they are superimposed with the dipole noise, the two are almost undistinguished. This suggests that the dipole source of trailing edge scattering dominates the installation noise generation at this observer's polar angle. These findings are further checked at higher polar angles, showing that the dipole source remains as the dominant mechanism of noise generation.

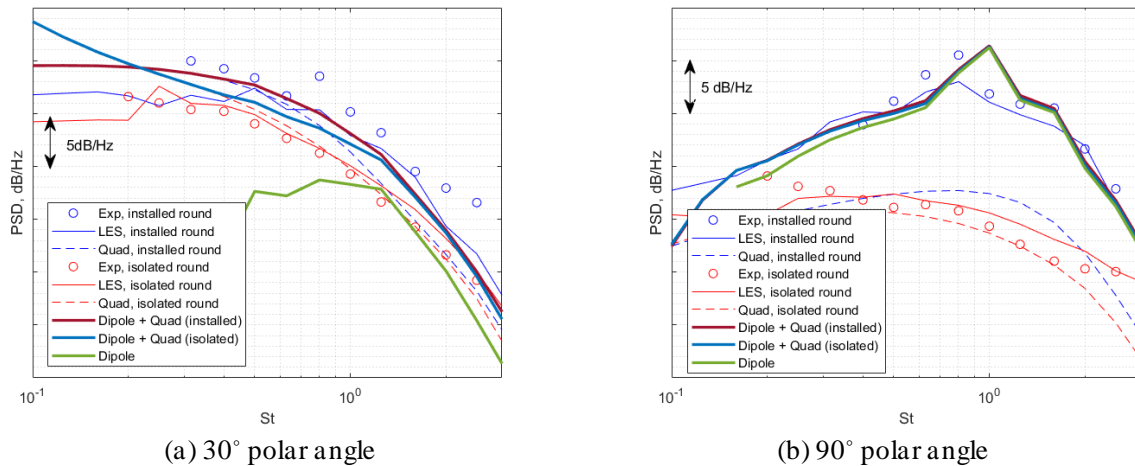


Figure 11 Far-field noise prediction of jet-wing configuration at the polar angle 30° and 90° under the wing

V. Conclusions

The sources of installed jet noise are decomposed into quadrupole sources due to turbulent mixing and dipole sources due to the unsteady loadings on the solid surface. Goldstein's acoustic analogy is employed to analyze the quadrupole source and predict its generated noise while trailing edge scattering of evanescent waves is used to approximate the dipole source and predict the emitted noise with the Amiet's approach. The two sources and their prediction method are first validated on a canonical jet-plate configuration, where the interactions between jet and wing barely modify the jet turbulence. Hence, the quadrupole source and noise of the installed jet remain almost the same as those of the isolated jet. The far-field noise is well predicted by adding the dipole noise and the quadrupole noise together. The validated methods are then applied to investigate the installation noise generation of a closely installed jet-wing configuration, where the turbulence downstream of the wing is significantly amplified by the jet-wing interactions. Consequently, the quadrupole sources are amplified as well. The results show that the increased quadrupole source dominates the installed jet noise generation at the polar angle of 30° under the wing. When the polar angle increases, the increased quadrupole noise due to the enhanced turbulence is not sufficient to explain the noise increase due to installation. The dipole source of trailing edge scattering plays a dominant role in producing the installation noise. This work clarifies the mechanisms of installed jet noise, especially for closely installed jet

configurations. It will provide an insightful guide for the design of efficient control strategies for reducing installed jet noise.

Acknowledgments

The ARCHER computing time is provided by the UK Turbulence Consortium under EPSRC grant EP/L000261/1 and PRACE Distributed European Computing Initiative. The simulation of jet-wing configuration was performed in the EU-funded project “JERONIMO” (ACP2-GA-2012-314692-JERONIMO). The authors would like to thank Drs Jack Lawrence and Anderson Proneca for providing the experimental measurement to validate the simulation of jet-plate configuration.

References

1. Pepper, C.B., M.A. Nascarella, and R.J. Kendall, *A Review of the Effects of Aircraft Noise on Wildlife and Humans, Current Control Mechanisms, and the Need for Further Study*. Environmental Management, 2003. **32**(4): p. 418-432.
2. Bushell, K., *Measurement and prediction of jet noise in flight*. AIAA aeroacoustics conference, 1975: p. AIAA 75-461.
3. Fisher, M., M. Harper-Bourne, and S. Glegg, *Jet engine noise source location: The polar correlation technique*. Journal of Sound and Vibration, 1977. **51**(1): p. 23-54.
4. Head, R.a.F., M., *Jet/surface interaction noise - analysis of far-field low frequency augmentations of jet noise due to the presence of a solid shield*. AIAA aeroacoustics conference, 1976: p. AIAA 76-502.
5. Mead, C.J. and P. Strange, *Under-wing installation effects on jet noise at sideline*. ROLLS ROYCE PLC-REPORT-PNR, 1999.
6. Williams, J.E.F. and L.H. Hall, *Aerodynamic sound generation by turbulent flow in the vicinity of a scattering half plane*. Journal of Fluid Mechanics, 1970. **40**(4): p. 657-670.
7. Lyu, B., A.P. Dowling, and I. Naqavi, *Prediction of installed jet noise*. Journal of Fluid Mechanics, 2017. **811**: p. 234-268.
8. Amiet, R.K., *Acoustic radiation from an airfoil in a turbulent stream*. Journal of Sound and Vibration, 1975. **41**(4): p. 407-420.
9. Pastouchenko, N. and C. Tam, *Installation Effects on the Flow and Noise of an Under-the-Wing Mounted Dual Stream Jet*. in *43rd AIAA Aerospace Sciences Meeting and Exhibit*. 2005.
10. Jameson, A., *Formulation of kinetic energy preserving conservative schemes for gas dynamics and direct numerical simulation of one-dimensional viscous compressible flow in a shock tube using entropy and kinetic energy preserving schemes*. Journal of Scientific Computing, 2008. **34**(2): p. 188-208.
11. Wang, Z.-N., et al., *Parallel computation of aeroacoustics of industrially relevant complex-geometry aeroengine jets*. Computers & fluids, 2019. **178**: p. 166-178.
12. Spalart, P.R. and S.R. Allmaras, *A one-equation turbulence model for aerodynamic flows*. Recherche Aerospaciale, 1994. **1**: p. 5-21.
13. Nicoud, F. and F. Ducros, *Subgrid-scale stress modelling based on the square of the velocity gradient tensor*. Flow, Turbulence and Combustion, 1999. **62**(3): p. 183-200.
14. Wang, Z.-N., et al., *Large-eddy-simulation prediction of an installed jet flow and noise with experimental validation*. AIAA journal, 2020. **58**(6): p. 2494-2503.
15. Tyacke, J., Z.-N. Wang, and P. Tucker, *LES-RANS of installed ultra-high bypass-ratio coaxial jet aeroacoustics with a finite span wing-flap geometry and flight stream - Part 1: round nozzle*. AIAA paper, 2017. **2017-3854**.
16. Tyacke, J.C., Z.-N. Wang, and P.G. Tucker, *LES-RANS of Installed Ultra-High-Bypass-Ratio Coaxial Jet Aeroacoustics with Flight Stream*. AIAA journal, 2019. **57**(3): p. 1215-1236.
17. Goldstein, M.E., *A generalized acoustic analogy*. Journal of Fluid Mechanics, 2003. **488**: p. 18.
18. Karabasov, S.A., et al., *Jet Noise: Acoustic Analogy informed by Large Eddy Simulation*. AIAA journal, 2010. **48**(7): p. 1312-1325.
19. Gryazev, V., A.P. Markesteijn, and S.A. Karabasov, *Generalized Acoustic Analogy Modeling of Hot Jet Noise*. AIAA journal, 2022. **60**(4): p. 2383-2396.
20. Wang, Z.-N., J.C. Tyacke, and P.G. Tucker, *LES-RANS Study of Serrated Nozzle Jet Aeroacoustics for an Installed Ultra-High-Bypass-Ratio Aeroengine*. AIAA journal, 2021. **59**(10): p. 4155-4165.
21. Schmidt, O.T., et al., *Spectral analysis of jet turbulence*. Journal of Fluid Mechanics, 2018. **855**: p. 953-982.
22. Jordan, P. and T. Colonius, *Wave Packets and Turbulent Jet Noise*. Annual Review of Fluid Mechanics, 2013. **45**(1): p. 173-195.